Soils and Rocks
An International Journal of Geotechnical and Geoenvironmental Engineering
www.soilsandrocks.com
ISSN 1980-9743
ISSN-e 2675-5475

# Evaluation of heat pump efficiency within an energy pile group: effect of heat cluster, underground seepage and seasonal cycles

Thibault Badinier[1], Badr Ouzzine[1], Jean de Sauvage[1#],
Philippe Reiffsteck[1]

Article

**Keywords**
Geothermal energy
Energy geostructures
Numerical modelling
Piles group
Heat pump efficiency

**Abstract**

Energy geostructures are a cost-effective solution for low enthalpy geothermal installations. Heat exchanger pipes are attached to the reinforcing cages of geotechnical structures to combine structural and geothermal roles. However, the installation of a group of multiple energy structures, such as a pile group, can lead to a heat cluster effect, which tends to decrease the efficiency of the heat pump (COP factor). This phenomenon is amplified by the number of grouped energy geostructures. However, energy geostructures are often installed in areas with groundwater flow. This induces a thermal washing effect, which decreases the risk of multi-year thermal shifts and preserves heat pump efficiency. In this paper, we evaluate the heat cluster effect in a group of piles, its influence on heat pump COP, the benefit of thermal washing due to underground water flow, and the effect of various seasonal scenarios. For this purpose, we present and use a specific numerical process that allows for modeling energy geostructure installations and interactions between groundwater flow models and thermal models. The heat pump COP is then estimated according to variable heat load, which depends on soil temperature.

## 1. Introduction

The demographic, climatic, and energy context has been pushing for several years now towards renewable and local energy solutions that curb our contribution to global warming. According to the International Energy Agency (IEA, 2022), the residential sector is the second-largest energy-consuming sector in France, accounting for around 25% of total energy consumption. However, only a small part (6%) of this energy is CO2-free. Consequently, the residential sector is also the second-largest emitter of greenhouse gases after the transport sector (see Figure 1).

Among the renewable energy solutions, energy geostructures have been developing for a few decades. Although there were only about 200 energy geostructures in service in 2018, the number of installations worldwide is increasing (Di Donna et al., 2020). Energy geostructures are a cost-effective, non-intermittent, and low-carbon way to heat or cool new buildings using a heat pump installation. Their implementation allows for the harvesting of local energy and does not present the same risk level as nuclear energy. Additionally, the use of a heat pump induces an electrification of the process, which makes it easily coupled with other renewable energy sources. Heat exchanger tubes are attached to the reinforcement cages of the geostructures, as shown in Figure 2a. A fluid circulates in the tube to draw heat from the soil in winter or to inject heat from the building into the soil in summer (see Figure 2b).

Energy geostructures come in multiple technical solutions (Laloui & Di Donna, 2013; Loveridge et al., 2020). The most ancient and commonly used are energy piles (Amatya et al., 2012; Brandl, 2006; Pahud, 2013; Yavari, 2014) because of their similarity with classical geothermal borehole energy drains. The available energy for such installations depends on the type of pile, depth, and soil condition. However, experimental data show an average heat drain capacity of around 80 W per meter of pile, according to (Loveridge et al., 2020). Nonetheless, other technical and more complex solutions exist, such as diaphragm walls (Brandl, 2006; Di Donna et al., 2017; Makasis & Narsilio, 2020) or tunnels (Barla et al., 2019; Frodl et al., 2010).

#Corresponding author. E-mail address: jean.de-sauvage@univ-eiffel.fr
[1]Univ Gustave Eiffel, Department Geotechnics, Environment, Natural Hazard, and Earth Science, Laboratory Soil Rocks and geotechnical Works – GERS-SRO, F-77454 Marne-la-Vallée, France

Submitted on May 30, 2024; Final Acceptance on October 7, 2024; Discussion open until May 31, 2025.
Editor: Renato P. Cunha
https://doi.org/10.28927/SR.2025.004224

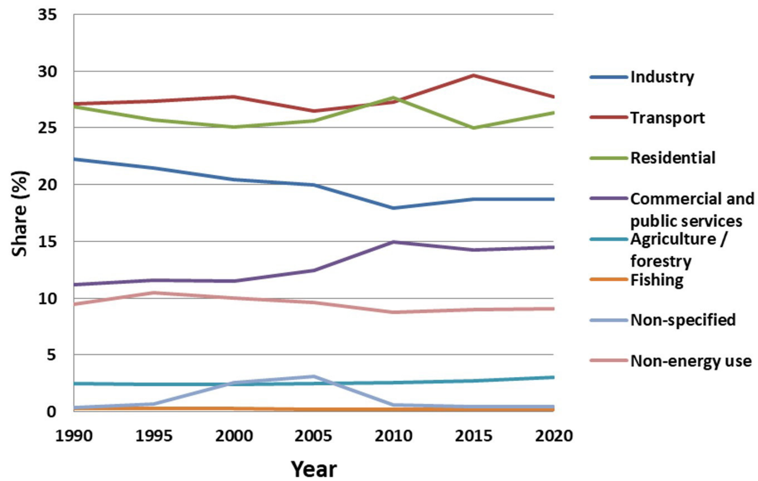


**Figure 1.** Energy consumption share in France by sector (based on data from (IEA, 2022)).

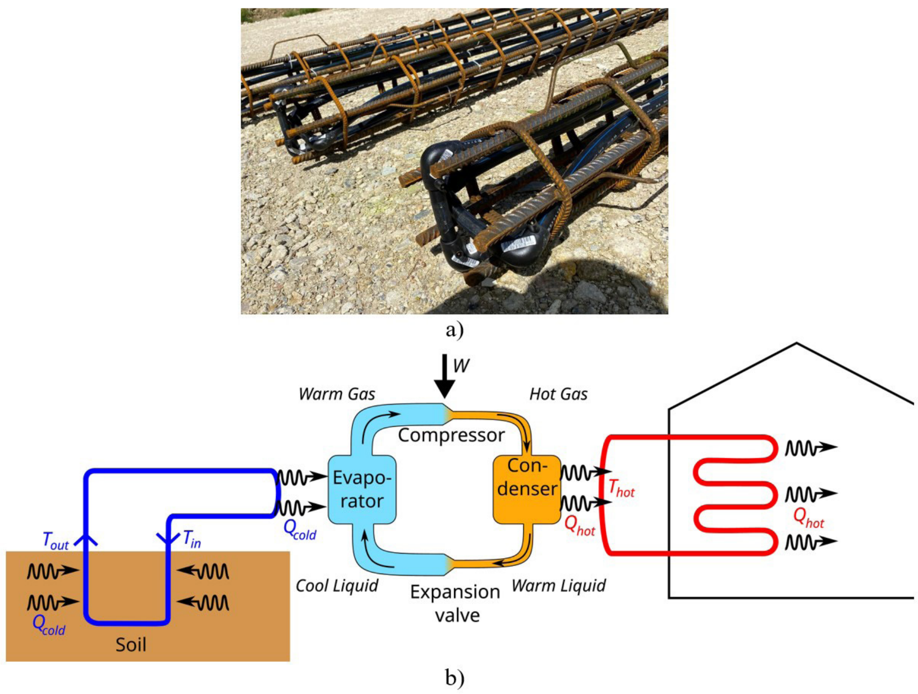


**Figure 2.** a) Example of reinforcement cage of and energy pile (photo from: University Gustave Eiffel); b) Schematic heat pump system.

Like other shallow geothermal systems, energy piles' operation benefits from the relatively constant temperature in the soil below a certain depth. This temperature represents a source of energy that can be moved from the soil to the building for heating purposes. The first law of thermodynamics states that heat naturally moves from hot to cold. Therefore, to move heat from the ground (around 13 °C) to the heating system of a building (around 35 °C), electric power is needed, which is provided by a heat pump. The ratio between the heat power provided to the building (noted $Q_{hot}$) and the electric power consumed (noted $W$) defines the performance factor of the system (noted COP) (Equation 1a). It's worth noting that, according to the first law of thermodynamics, the heat power is the sum of the power drained from the soil (noted $Q_{cold}$) and the electrical power transformed into heat (Equation 1b).

$$\text{COP} = \frac{Q_{hot}}{W} \tag{1a}$$

$$Q_{hot} = Q_{cold} + W \tag{1b}$$

In winter conditions, the operation of the heat pump will drain heat power from the soil, thereby decreasing the soil temperature. This temperature variation in the soil is called thermal anomaly. On one hand, such thermal anomaly will have an influence on structural mechanics (Amatya et al., 2012;

Bourne-Webb et al., 2016; CFMS, 2017; Maghsoodi, 2020; Mimouni & Laloui, 2015). On the other hand, it will affect the heat pump efficiency (COP factor). Indeed, according to (Pahud & Lachal, 2004), considering a constant heat power demand in the building, the bigger the temperature difference between the ground and the heating system, the more electrical power the heat pump must provide to move heat energy from the cold source to the hot source, thereby reducing the COP factor at the same time. This effect could be quantified according to (Staffell et al., 2012) by benchmarking the technical specification of numerous heat pump systems (see Figure 3). Therefore, during the winter season, the soil temperature reduction will decrease the heat pump efficiency.

Furthermore, energy piles are commonly built in groups for structural purposes, therefore several energy piles might draw their energy from the same thermal reservoir. In such cases, the thermal anomaly of each pile will have a cumulative effect on the global efficiency, decreasing the COP factor. In the case of pile groups, one can expect that the effect of thermal clusters will increase while the piles are built closer to each other (Di Donna et al., 2016; Lou et al., 2021). According to (Fujii et al., 2005), the optimal distance between two geothermal sources should be 3 to 6 m. However, according to French and European design rules (Brach et al., 2014; Burlon et al., 2017), inside pile groups the distance between two piles should be less than 3 diameters, i.e., around 2 m.

Building energy piles below the water table can have a significant impact on the thermal behavior of the system. Firstly, in saturated conditions, the thermal conductivity of the soil is greater, making it easier to harvest thermal energy (Abu-Hamdeh, 2003; Fromentin & Pahud, 1997). Secondly, the underground water flow affects the temperature field in the soil. Seepage in the soil displaces the thermal anomaly downstream, a phenomenon known as thermal advection, which can help to avoid the thermal anomaly by renewing the water around energy geostructures, producing a thermal washing effect (Badinier et al., 2023; Lou et al., 2021). However, as it also moves the thermal anomaly downstream, it could have an impact on the behavior of other energy geostructures (Badinier et al., 2022; Barla et al., 2018; de Sauvage et al., 2020; Ouzzine et al., 2023). Finally, the presence of geostructures might disturb the water flow, creating a dam effect which could decrease the thermal washing of the system (Attard et al., 2016; Delerablée, 2019).

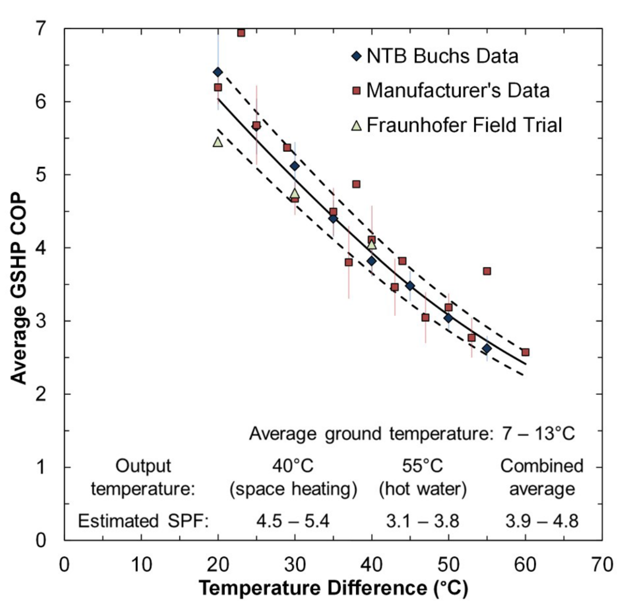


**Figure 3.** Benchmarked COP factor regarding temperature difference between hot and cold source for ground sourced heat pump (Staffell et al., 2012).

During summer, energy geostructures can also be used as an economical solution for building cooling systems (Anstett et al., 2005; Brandl, 2006). Therefore, the thermal behavior is inverse, and the system aims at transferring the excess thermal energy from the building to the soil via the geostructure. Whereas, in winter conditions, the soil temperature is always cooler than the target temperature inside the building, the use of a heat pump is not systematic in summer conditions. Indeed, while the average soil temperature is around 13 °C and the coolant fluid target could be set to 15 °C, the heat transfer will occur naturally without heat pump activation. This condition is called "free cooling". This effect will be enhanced if the soil temperature has been cooled. In opposition, if the soil temperature rises over the coolant fluid temperature, the heat pump will be needed to transfer the heat energy. In such "active cooling" conditions, the hot source will be the building and the cold source will be the soil (Allaerts et al., 2015; Fadejev et al., 2016, 2017; Pahud & Hubbuch, 2007). In any case, the cooling operation of the building will produce heat exhaust in the soil around the energy geostructure, increasing soil temperature, and recharging the heat reservoir. Therefore, seasonal use is profitable as it helps to avoid multi-year thermal shifts and higher soil temperatures will allow heat pumping with higher efficiency (smaller cost).

To summarize the problem, drawing heat from the ground using a group of energy piles leads to a decrease in soil temperature, which in turn reduces the efficiency of the heat pump system (COP factor). This effect may depend on the geometry of the group, particularly the distance between the piles. On the other hand, groundwater may create a thermal washing effect, reducing the thermal anomaly and restoring the efficiency of the heat pump system. This phenomenon will be greater as the seepage velocity increases. Finally, in summer mode, the heat evacuation in the soil will restore the thermal reservoir, providing heat energy for the winter season at a higher temperature, which will increase the COP factor.

The first elements of answer to this problem can be found in the literature: complex numerical models are developed to consider the thermal behavior of the heat pump (Cui & Zhu, 2018; Gultekin et al., 2016). These models capture the dependence of COP on soil temperature, evolving over time, but they do not consider the groundwater flow. (Li et al., 2018) adapted such a model to study the impact of groundwater flow but focused on one pile, allowing to characterize the washing effect but not the group behavior. On the contrary studies have been carried out on the energy performance of a Borehole Heat Exchanger field in the presence of a groundwater flow (Lazzari et al., 2010; Zanchini et al., 2012) but they do not include a proper dependency of the heat pump COP on the soil temperature. Generally, the performance of the heat pump is evaluated a posteriori by correlation with the temperatures calculated in the ground. Therefore, the simulations are not coupled and the thermal loads on heat exchangers are assumed rather than calculated. Actually, a complete literature review (Zhao et al., 2022) highlighted that no existing study offers a proper characterization of the interaction between groundwater flow and unbalanced heat demand, considering the COP dependency on the soil temperature.

In this study, thermal efficiency questions are addressed by examining the theoretical thermal behavior of the heat pump system depending on the geometry of the pile group, the underground water flow conditions, and the seasonal heating and cooling cycles. For this purpose, numerical models using the FEM software CESAR-LCPC are developed to simulate this problem of hydro-thermal coupling.

This paper aims to present the capabilities of this new numerical process and to provide a first realistic evaluation of heat pump efficiency for a group of energy piles, quantifying the effects of heat clustering and thermal washing.

## 2. Numerical model

For this study, we utilize CESAR-LCPC, a finite element modeling (FEM) software continuously developed by the University Gustave Eiffel. This software is specifically designed for civil engineering problems, such as foundations, embankments, concrete structures, etc. (Humbert et al., 2005). Notably, it possesses the capability to handle transient diffusion problems, including thermal and hydraulic issues. This feature enables the study of geothermal problems while considering groundwater flow conditions. Furthermore, the CESAR-LCPC software can be employed with a Python script and the dedicated Python module known as "Pilote CESAR". With this tool, one can describe model geometry, meshing, boundary conditions, and loading, run computations, and analyze resulting data. Other Python modules can also be incorporated within the script. Consequently, it facilitates easy parametric studies, even regarding geometrical aspects.

### 2.1 Numerical problems and equations

We aim to solve simultaneously the hydraulic problem, *i.e*, seepage velocities, and the thermal problem, *i.e.*, the temperatures field. We assume that the hydraulic problem involves water flow in fully saturated soils. The governing equation is the classical Darcy Equation 2:

$$\vec{v} = -k \cdot \overrightarrow{grad}\, h \text{ and } div\, \vec{v} = 0 \tag{2}$$

where $\vec{v}$ is the Darcy water velocity in $\mathrm{m \cdot s^{-1}}$, $k$ is the water permeability in $\mathrm{m \cdot s^{-1}}$ and $h$ is the hydraulic load in m.

The thermal problem is governed by the heat Equation 3:

$$C_v \frac{dT}{dt} + div\vec{j} = 0 \tag{3}$$

where $T$ the temperature in $\mathrm{K}$, t is the time in s, $\vec{j}$ is the total heat flux in $\mathrm{W}$ and $Cv$ is the volumetric thermal capacity in $\mathrm{W \cdot s \cdot m^{-3} \cdot K^{-1}}$ (note we consider here the total heat capacity of the saturated soil).

In underground conditions, the heat flux is the sum of two fluxes, each corresponding to a distinct physical phenomenon.

Firstly, the conductive flux, noted $\vec{j}_{cond}$, is due to natural thermal conduction and computed according to Fourier Law, considering $\lambda$ the thermal conductivity in $\mathrm{W \cdot m^{-1} \cdot K^{-1}}$, and the temperature gradient (Equation 4):

$$\vec{j}_{cond} = -\lambda\, \overrightarrow{grad}\, T \tag{4}$$

Secondly, the advection flux, noted $\vec{j}_{adv}$, corresponds to the movement of underground water with its stored energy. It is computed by considering underground waterflow velocity $\vec{v}$ according to Darcy's Equation 2, the water volumetric heat capacity noted $C_{v,w}$ and $T$ the temperature (Equation 5)

$$\vec{j}_{adv} = \vec{v}\, C_{v,w}\, T \tag{5}$$

Therefore, the thermal problem depends on the hydraulic results, making the global problem coupled. However, we assume that the variation of temperature is not significant enough to change the water viscosity or to freeze the soil. As a result, the effect of temperature on the hydraulic problem is considered negligible and is not considered in the numerical process.

### 2.2 Variable heat loading

The principle of the heat pump is represented on Figure 2b. In winter mode, the system extracts a quantity of heat energy $Q_{cold}$ in the cold source (in this case the soil), and delivers a quantity of heat energy $Q_{hot}$ to the building, while consuming a quantity $W$ of electric power. To do so, a fluid, with a volumetric thermal capacity $C_{v,f}$, is pumped in the piles heat exchangers at a pumping rate $q$ ($\mathrm{m^3 \cdot s^{-1}}$), resulting in a temperature difference between the inlet and outlet fluid (. $T_{in}$ and $T_{out}$). Overall, it produces heating fluid at temperature $T_{hot}$.

As previously explained, the relationship between $Q_{cold}$, $Q_{hot}$ and $W$ is given by the first law of thermodynamics (see Equation 1b) and the heat Pump efficiency is defined as the COP factor (see Equation 1a). Therefore, $Q_{cold}$, should be computed according to Equation 6.

$$Q_{cold} = Q_{hot}\left(1-\frac{1}{\mathrm{COP}}\right) \tag{6}$$

However, according to the manufacturer's data, the heat pump efficiency will decrease as the temperature gap between the cold and hot sources increases. Based on their benchmarking work (see Figure 3) (Staffell et al., 2012) propose the Equation 7 to compute the COP factor, depending on the temperature lift between the hot circuit (on the builing side), with temperature $T_{hot}$, and the cold circuit (on the soil side), with the temperature $T_{cold}$ expressed in $K$:

$$COP = 8.77 - 0.150\left(T_{hot} - T_{cold}\right) + 0.000734\left(T_{hot} - T_{cold}\right)^2 \tag{7}$$

While the hot circuit temperature is a given data according to the building heating system (around 35 °C), the cold circuit temperature depends on the soil temperature ($T_{soil}$), the exchanged power inside the soil ($Q_{cold}$), the geostructure fluid pumping rate, ($q$ in $\mathrm{m^3 \cdot s^{-1}}$), and the fluid's volumetric heat capacity ($C_{\mathrm{v,f}}$).

To exchange $Q_{cold}$ with the soil, the heat pump circulates the geostructure's fluid with a difference between the inlet temperature $T_{in}$ and the outlet temperature $T_{out}$. $Q_{cold}$ is then computed with Equation 8a. Meanwhile, we consider that the same amount of energy is extracted from the soil through the pile and is computed according to a simple thermal resistive equation (see Equation 8b). Here, $T_{fl}$ is the average fluid temperature computed with Equation 8c and $R_{th}$ is the thermal resistance of the pile in $\mathrm{K \cdot W^{-1}}$ (evaluated numerically, see section 4.1).

$$Q_{cold} = C_{v,f} \cdot q \cdot \left(T_{out} - T_{in}\right) \tag{8a}$$

$$Q_{cold} = \frac{T_{soil} - T_{fl}}{R_{th}} \tag{8b}$$

$$T_{fl} = \frac{T_{in} + T_{out}}{2} \tag{8c}$$

By combining Equations 8a, 8b and 8c, and assuming that cold circuit temperature $T_{cold}$ is equal to $T_{in}$, we obtain the following equation:

$$T_{cold} = T_{in} = T_{soil} - Q_{cold} \cdot R_{th} - \frac{Q_{cold}}{2C_{v,f} \cdot q} \tag{9}$$

Finally, by combining Equations 6, 7 and 9, we obtain the following equation:

$$COP = 8.77 - 0.150\left[T_{hot} - T_{soil} + Q_{hot}\left(1-\frac{1}{COP}\right)\left(R_{th} - \frac{1}{2C_{v,f} \cdot q}\right)\right] + 0.000734\left[T_{hot} - T_{soil} + Q_{hot}\left(1-\frac{1}{COP}\right)\left(R_{th} - \frac{1}{2C_{v,f} \cdot q}\right)\right]^2 \tag{10}$$

Finally, considering $T_{hot}$, $C_{v,f}$, $q$, and $R_{th}$ as constants of the system and $Q_{hot}$ as an input data, the COP factor is the solution of a third-degree polynomial equation, depending only on soil temperature ($T_{soil}$).

**2.3 Summer mode heat pump**

In summer mode, the behavior of the system is inverse. Therefore, the heat pump aims at moving calories from the cold source (now the building) to the hot source (now the soil). The efficiency of the heat pump in summer mode, noted as $\mathrm{COP}_S$, is then measured as the ratio between the heat evacuated from the building $Q_{cold}$ and the consumed electric power $W$. Considering Equations 1a, 1b and 7:

$$COP_S = \frac{Q_{cold_S}}{W} = \frac{Q_{hot_S} - W}{W} = COP - 1 = 7.77 - 0.150\left(T_{hot_S} - T_{cold_S}\right) + 0.000734\left(T_{hot_S} - T_{cold_S}\right)^2 \tag{11}$$

However, in the case of free cooling, the difference between $T_{hot_S}$ and $T_{cold_S}$ could be small or even negative, which is outside the dataset of (Staffell et al., 2012). Nevertheless, for this study, we assume the validity of this equation even for negative temperature gaps for three main reasons. Firstly, for numerical continuity of the computing process during summer period modelling. Secondly, because the $\mathrm{COP}_S$ remains defined as the heat pump continues to consume energy due to circulating pumps. Thirdly, because at such temperature gaps, the efficiency of the heat pump is high enough to consider the error on $W$ estimation as negligible.

Finally, in summer mode, the imposed heat to the soil is $Q_{hot_S}$ which is computed with Equation 12.

$$Q_{hot_S} = Q_{cold_S}\left(1+\frac{1}{\mathrm{COP}_S}\right) \tag{12}$$

# 3. Global computation process

The global computation process is described below and can be summarized with Figure 4. First, the hydraulic problem is described, including geometry, parameters, boundary conditions, and loading. The computation is conducted to obtain a steady-state solution using the DTNL (Diffusive Transient, Non Linear) solver from CESAR-LCPC (Piau et al., 2005). The results are stored and will be used in the thermal computations.

Secondly, the thermal problem is described with geometry, parameters, and boundary conditions. The computation is conducted as a transient evolution on successive time steps (t) using the DTNL solver from CESAR-LCPC. In transient mode, this solver uses implicit Eulerian integration, which ensures stability of the results, independently of the time step. The initial temperature of the entire system is assumed to be homogeneous at 13 °C. At each computation step, the

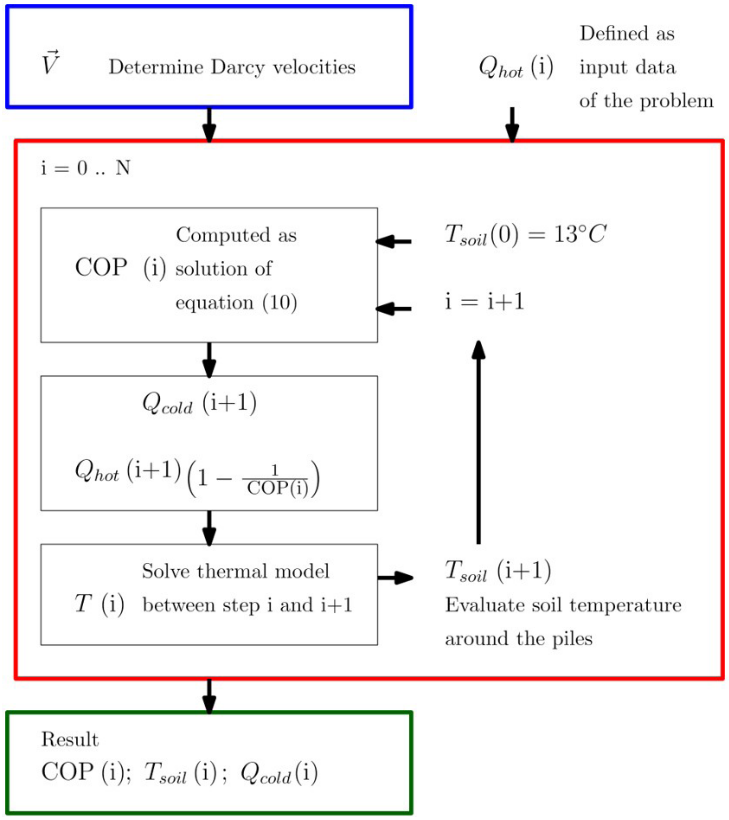


**Figure 4.** Schematization of the program process.

thermal loading imposed on the model, $Q_{cold}$, is modulated according to the COP factor computed through Equation 10 considering the current soil temperature.

In particular, for the first step, the COP factor is computed based on the initial temperature by solving Equation 10. Then, the thermal loading is determined based on Equation 6 and the values of $Q_{hot}(t)$ given as input data of the problem.

After step $t = i$, the average soil temperature around the piles is determined from the temperature results. The $\text{COP}(i)$ at time $t = i$ is then computed. This value is used to compute the $Q_{cold}(i+1)$, the thermal loading imposed on the model between step $i$ and $i+1$. The computation between step $t = i$ and step $t = i+1$ then proceeds. The computation process continues like this until the defined time $t = N$.

At the end of the process, the successive values of $\text{COP}(t)$, $T_{soil}(t)$ and $Q_{cold}$ are stored in a .txt file. The temperature field evolution can be observed and studied using CESAR-LCPC tools.

In cases of seasonal summer and winter solicitation, the program is able to switch from winter COP computation to summer $\text{COP}_S$ computation. Therefore, in summer mode, the values of imposed heat to the building, $Q_{hot}(t)$, become negative, and the sign of the heat loading, $Q_{cold}$, imposed on the model also changes (corresponding respectively to $Q_{cold_S}$ and $Q_{hot_S}$ from Equation 12).

## 4. Study case description

For the purpose of this study, we produce models based on the case of a fictitious building of $1000\,m^2$ requiring a peak heating power of $15500\,W$. The building is therefore built on a group of 20 energy piles, each 12 m long. These values have been established based on the example of a neutral energy building in Gonesse, France (CFMS, 2022).

### 4.1 Geometry

The piles are 12 m long. Therefore, we assume an invariable behavior along the piles, and we will use a 2D model of the pile group. The distance between the piles will be part of the parametric study, varying from 1 diameter to 10 diameters. The global size of the model is six times longer than the pile group (at least 20 m long), and three times larger (at least 10 m wide). The pile group is in the middle of the left half of the model, and the underground flow goes from left to right. These geometric conditions have been chosen to limit interaction between the group and the boundary condition, including the thermal plume formation. The principles of these models are shown on Figure 5a.

Each pile is assumed to have a diameter of 0.60 m, and to be equipped with four heat exchanger tubes attached to the reinforcement cage on the side of the pile. In order to save

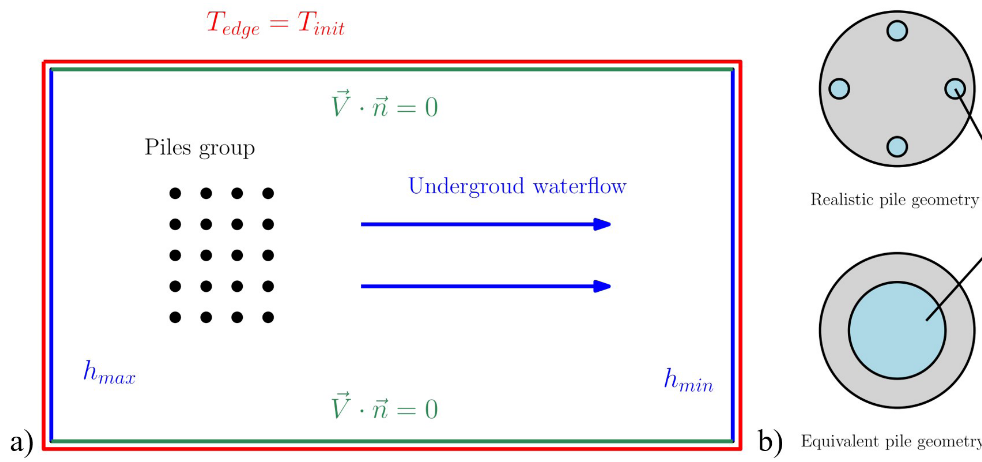


**Figure 5.** a) Schematic description of the model; b) Equivalent pile geometry.

**Table 1.** Models' parameters.

| | Thermal conductivity | Vol. Thermal capacity | Pile behavior |
|---|---|---|---|
| | $\lambda$ ($W \cdot m^{-1} \cdot K^{-1}$) | $C_v$ ($J \cdot m^{-3} \cdot K^{-1}$) | $k$ ($m \cdot s^{-1}$) |
| Soil | 2.5 | 1.80 .10$^6$ | 10$^{-4}$ |
| Concrete | 1.8 | 1.80 .10$^6$ | 0 |
| Tube | 10$^{10}$ | 1.80 .10$^6$ | 0 |

computation time, such a level of detail is simplified using a unique central heat exchanger tube of greater diameter (as shown in Figure 5b). This simplified geometry is commonly used as it exhibits similar macroscopic thermal behavior. The radius of the equivalent tube is set to expose the same permanent thermal resistance as the realistic geometry (Cecinato & Loveridge, 2015). The pile thermal resistance is estimated using a numerical model that employs a detailed pile geometry, including the tube, concrete, fluid, etc. A heat flux is imposed between the tube and soil at a constant temperature. The temperature gap between the soil and tube is then used to compute the thermal resistance and, subsequently, the equivalent tube radius. In the study case, this equivalent radius has been numerically estimated to 0.19 m.

### 4.2 Parameters

For simplification purposes, the materials are assumed to be homogeneous and isotropic. All parameters are summarized in Table 1. For the hydraulic models, parameters are set to represent permeable soil and impermeable structures. Exact values do not impact the results as boundary conditions are set to obtain the targeted average Darcy velocities.

The thermal parameters of the materials are obtained from (Delerablée, 2019), which were evaluated on the experimental site of Sense City using a thermal probe test. As a particularity, the thermal conductivities of the tube are set to extremely high values in order to represent moving and turbulent fluid, which will result in a homogeneous temperature. However, the thermal capacity is set equal to that of the concrete to maintain the global thermal capacity of the pile constant.

The other parameters including heat pump parameters are listed below:

- Water volumetric thermal capacity: $C_{v,w} = 4.20 \cdot 10^6\ J \cdot m^{-3} \cdot K^{-1}$
- Fluid volumetric thermal capacity: $C_{v,f} = 3.67 \cdot 10^6\ J \cdot m^{-3} \cdot K^{-1}$
- Fluid pumping rate: $q = 3\,m^3 \cdot h^{-1}$
- Winter hot source temperature: $T_{hot} = 40^\circ C$
- Summer cold source temperature: $T_{cold_S} = 11^\circ C$
- Initial model temperature: $T_{init} = 13^\circ C$

### 4.3 Hydraulic model

The hydraulic model is set to impose an average underground water velocity, $V$, parallel to the model axis. Therefore, the upstream and downstream boundary conditions are set with imposed hydraulic charges. On the two other edges of the model, the boundary conditions are set to impose water velocities parallel to the model's edge. The difference between $h_{max}$ and $h_{min}$ is then computed according to Equation 13 with $L$ being the length of the model and proper conversion between $m \cdot s^{-1}$ and $m \cdot day^{-1}$. The hydraulic model boundary conditions are presented on Figure 5a.

$$h_{max} - h_{min} = \frac{V \cdot L}{k \cdot 86.4 \cdot 10^3} \tag{13}$$

### 4.4 Thermal model

The thermal boundary conditions are set to represent the soil temperature away from the thermal anomaly induced by the system. Therefore, the edge temperature is set to 13 °C, which is also the initial model temperature. The thermal loading is set as a cooling power imposed inside the tubes by the heat pump system. Its value is variable during the computation, as explained in Section 2.2. The imposed thermal load is computed to match the global heating need of the building and is equally shared between each pile and along the pile. The thermal model boundary conditions are presented in Figure 5a.

## 5. Parametric study and results

In this section, we present several parametric studies with diverse scenarios in order to demonstrate different behaviors of the system.

### 5.1 Group of pile under one month of peak use

For these first models, the scenario is one month of winter solicitation at the peak maximal heating power of $15.5\,\mathrm{kW}$. We also consider a daily activation pattern, with 12 h of heat pump activation and 12 h of rest ($0\,\mathrm{W}$ heating). The computation process uses 336 steps of 2 hours (28 days total), which allows for a detailed description of the heat pump behavior within each day.

This hypothetical heating scenario has been selected because it allows us to highlight the behavior of our heat pump model while keeping the temperature and $COP$ values within a realistic range. It is supposed to represent the maximal usability of the system in cases of peak heating need.

#### 5.1.1 Influence of seepage water velocities

The first study aims to observe the $COP$ evolution over 28 days of intensive use with different underground seepage velocities. For this case, the inter-pile distance is constant and equal to 3 diameters. The velocity range is then set between $0\,\mathrm{m \cdot day^{-1}}$ and $2.0\,\mathrm{m \cdot day^{-1}}$. Such a range has already been proven to be wide enough to observe various behaviors (Badinier et al., 2023).

As preliminary results, we can observe the final temperature fields with two different values of seepage velocities (Figure 6). We can observe that for a null seepage velocity, the thermal anomaly is concentrated on the piles group. In contrast, a relatively fast seepage results in a thermal plume and a smaller temperature decrease overall.

a)

b)

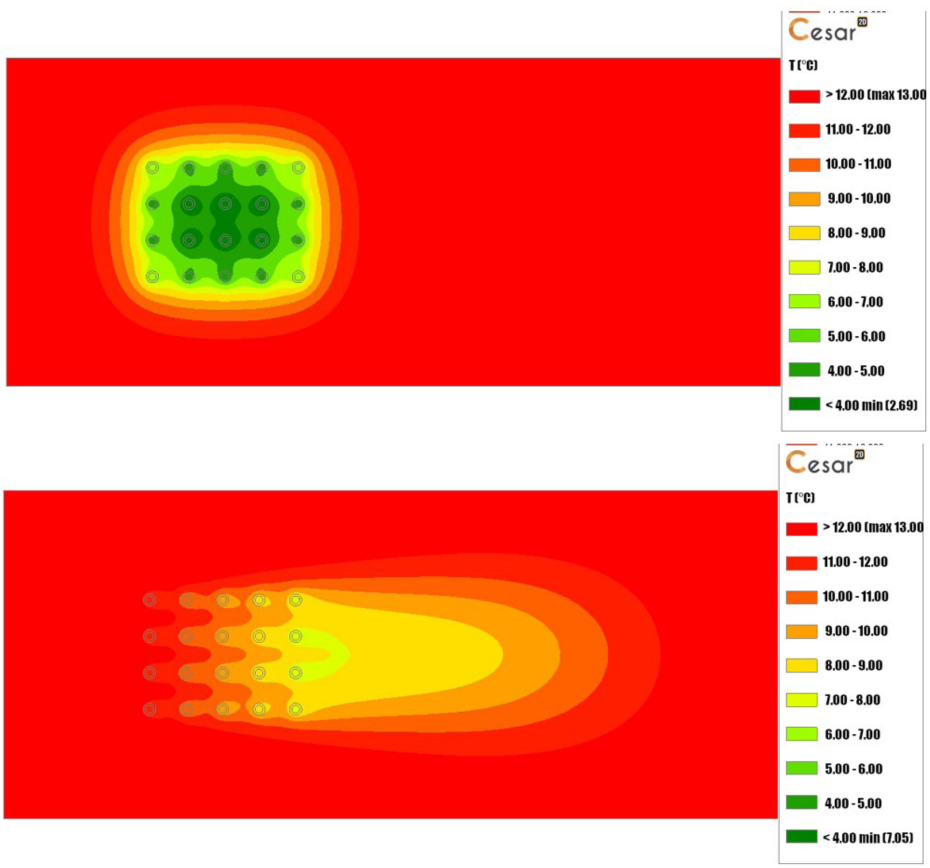


**Figure 6.** Temperature fields for different seepage velocities (a – 0 m.day$^{-1}$; b – 0.3 m.day$^{-1}$) and inter-pile distance of 1.2 m.

Figure 7a shows the COP evolution over the 28 days resulting from the computation process. As expected, the COP factor decreases over the period. However, the intermittency in the heat demand generates the particular wavelet shape of the curve, with decreasing values in activation periods and an increase of the COP during the resting period. The observation of the soil temperature data leads to the same observation. Indeed, according to Equation 10, these data are strongly linked. As an example, in case of average velocities of $0.3\,\mathrm{m \cdot day}^{1}$ the soil temperature decreases over the month from 13 °C to 9.9 °C. In contrast, with null seepage velocity, the average soil temperature will reach a minimum value of 4.5 °C.

As expected, the higher the water velocity, the higher the $COP$ value. For relatively low seepage velocities ( $0\,\mathrm{m \cdot day}^{-1}$ to $0.1\,\mathrm{m \cdot day}^{-1}$ ) the $COP$ does not stabilize and should tend to 1 for hypothetical infinite simulation. On the contrary, above a certain seepage velocity, the $COP$ stabilizes around an acceptable value. This phenomenon can easily be explained by the equilibrium between the input heat power by the inflow and the heat power drained by the heat pump system. The soil surrounding the energy piles is therefore maintained at a certain temperature that allows for acceptable efficiency of the heat pump.

The conclusion of this first study is consistent with our previous work (Badinier et al., 2023) and with the literature.

### 5.1.2 Influence of the inter-pile distance

The second study aims to observe the $COP$ evolution over the same period of time with different distances between the piles. The inter-pile distance is then set between 2 diameters and ten diameters. The seepage velocity is set to a constant value of $0.2\,\mathrm{m \cdot day}^{-1}$ .

Figure 7b shows the $COP$ evolution for the different inter-pile distances. The results tend to demonstrate the existence of a cluster effect. If multiple energy piles are close enough, they will all drain energy from the same soil area, and the thermal anomalies will have a cumulative effect. Therefore, a greater distance between piles will maintain the $COP$ at higher values.

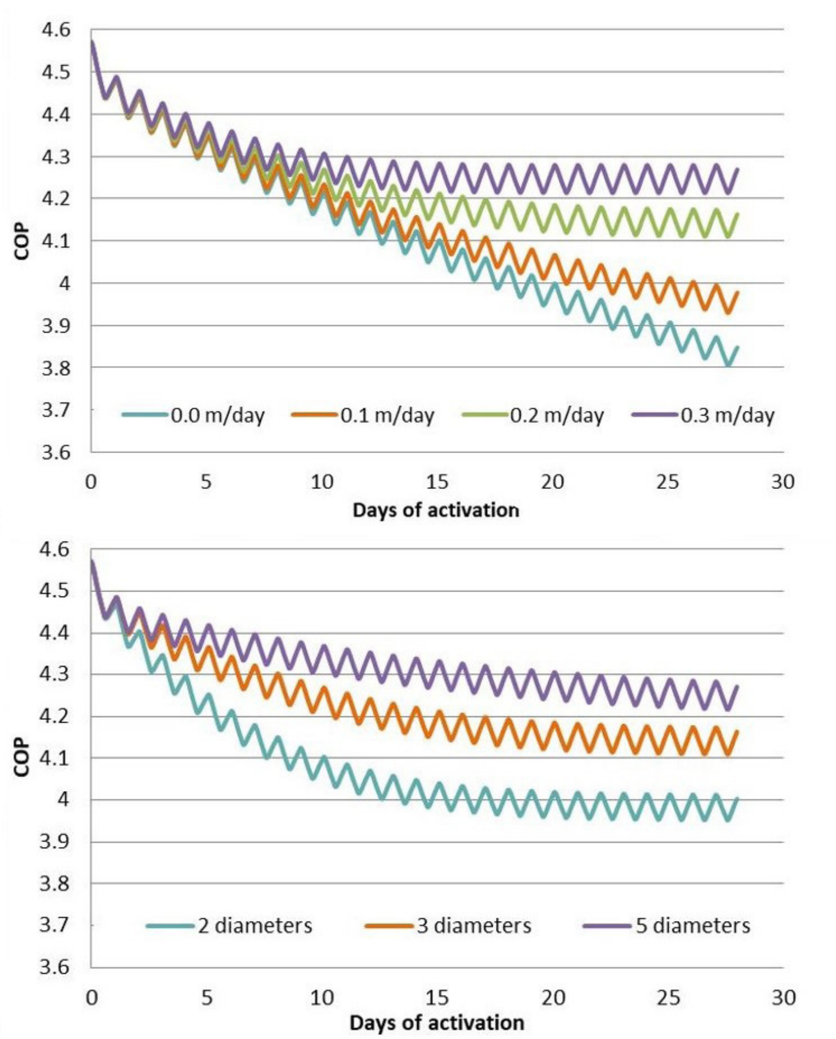


**Figure 7.** a) COP evolution for different seepage velocities; b) COP evolution for different inter-pile distances.

### 5.1.3 Overall study and results

Finally, with this heating scenario, we conduct all cases with different inter-pile distances and seepage velocities. Then we compare $\mathrm{COP}$ values after the 28 days as an indicator of the residual efficiency of the system in these cases. Note that the $\mathrm{COP}$ values presented here do not always correspond to a stable behavior, particularly for lower seepage velocities. The results are shown in Figure 8a.

This figure shows the combined effect of both seepage and inter-pile distance. As previously observed, for the same inter-pile distance, the efficiency will grow with the seepage velocities. This effect is observed for each value of inter-pile distance, but is stronger for smaller distances. Consistently, for the same seepage velocity, a greater distance results in higher $\mathrm{COP}$ final value. However, for seepage velocities over $0.5\,\mathrm{m}\cdot\mathrm{day}^{-1}$, the effect of the distance is almost negligible. The same conclusion could be drawn for summer mode. The $\mathrm{COP}_s$ values after 28 day of activation are shown in Figure 8c.

Based on the obtained $\mathrm{COP}$ and $\mathrm{COP}_s$ data, we propose the Equation 14 to evaluate the $\mathrm{COP}$ and $\mathrm{COP}_S$ depending on the inter-pile distance $D$ (in $\mathrm{m}$) and seepage velocity $V$ (in $\mathrm{m}\cdot\mathrm{day}^{-1}$):

$$\mathrm{COP}(D,V) = \mathrm{COP}_{max}\left(1 - \frac{0.3}{D}(1 - \exp(-3.8V)\right) \quad (14)$$

The comparison between data and formula is shown in Figure 8b and 8d. We were able to fit the same equation to both scenarios, only changing the target $\mathrm{COP}$ value with $\mathrm{COP}_{max} = 4.50$ and $\mathrm{COP}_{S,max} = 7.13$. This might indicate that this formula is applicable to this system independently of the solicitation scenario. However, further studies should be conducted to confirm the applicability to other system configurations.

Finally, we can conclude that distance between the piles and seepage velocity are favorable parameters for the heat pump efficiency. Therefore, each one of these parameters could be used to impact the $\mathrm{COP}$. As an example, in a case where the seepage velocity is small, the heat cluster effect can be tampered by increasing the inter-pile distance. We also notice that the seepage velocity impact is exponential. Since this parameter is measured with a high variability on real sites, great caution should be used in the design phase.

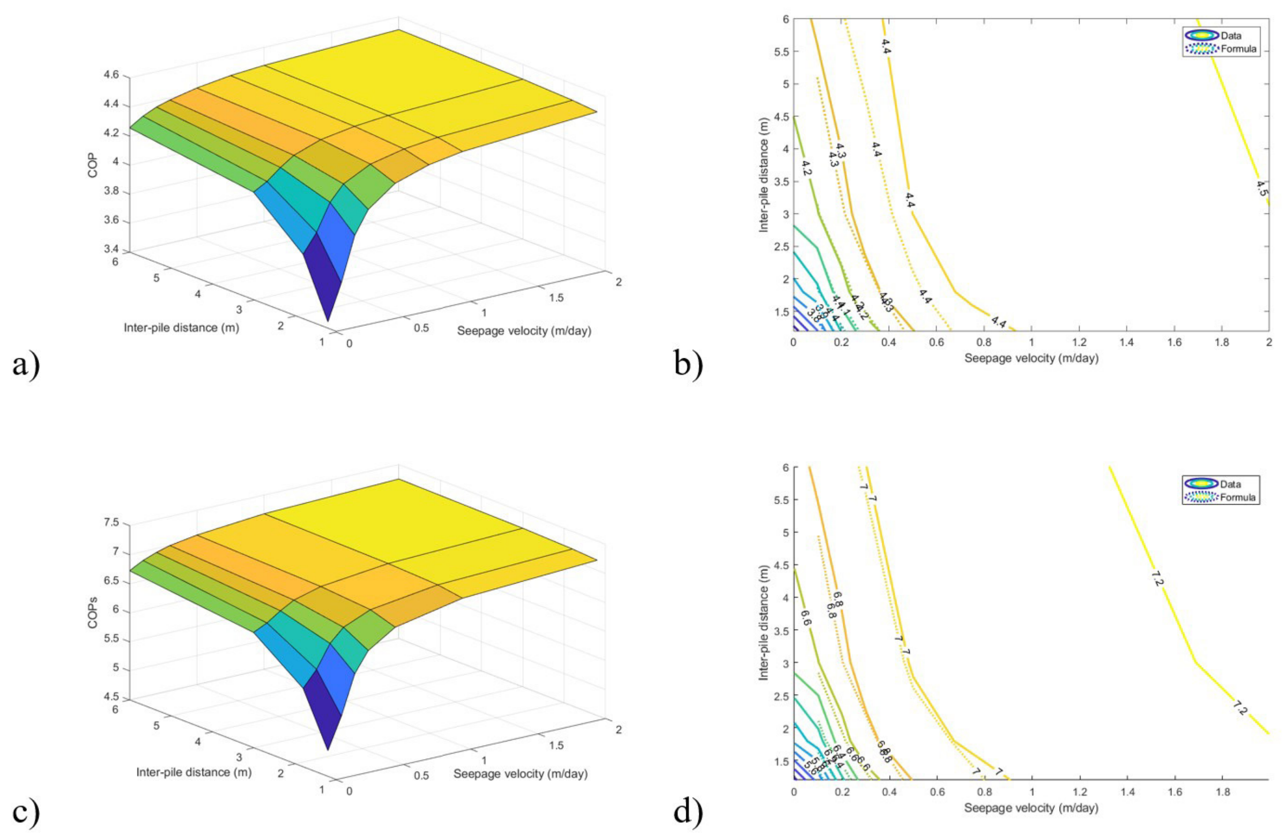


**Figure 8.** Comparison between computed $\mathrm{COP}$ and $\mathrm{COP}$ evaluated with the proposed formula. a) $\mathrm{COP}$ after 28 days on winter mode, depending on inter-pile distance and seepage velocities; b) Comparison between computed $\mathrm{COP}$ and evaluated $\mathrm{COP}$ with proposed formula; c) $\mathrm{COP}_S$ after 28 days in summer mode, depending on inter-pile distance and seepage velocities; d) Comparison between computed $\mathrm{COP}_s$ and evaluated $\mathrm{COP}_s$ with proposed formula.

### 5.2 Multi-year seasonal behavior

For this second model, the geometry is set to an inter-pile distance of 1.2 m (2 diameters), and the total size of the model is increased to twice the original size to ensure correct behavior at the model boundary for longer solicitation. The computation is set on 3649 steps of 12 hours, which represents a total of 5 years of use. The thermal solicitation is set to represent seasonal heating and cooling demand with sinusoidal variation. The peak heating demand is set to $15.5\,\text{kW}$ and the cooling demand depends on the case study, varying from 0% of the peak heating (only heating scenario) to 100% (symmetrical demand). The heating and cooling demand scenarios are presented in Figure 9. Note that setting the cooling in summer results in negative heat demand on the graph. In each case, the heating scenario uses a daily activation pattern of 12 h and 12 h rest. Two seepage conditions are compared: $0\,\text{m}\cdot\text{day}^{-1}$ and $0.4\,\text{m}\cdot\text{day}^{-1}$.

For these models, we aim to observe the behavior of the system through multiple years with various seasonal activation patterns and different seepage conditions.

Results of $COP$ and $COP_S$ values without seepage are presented on Figure 10a. Note that discontinuities of the $COP$ values are due to the shifts between summer and winter mode. With these results, we can observe multiple aspects of multi-year use of energy geostructures and heat pump. First, in case of totally unbalanced heating demand (0% building cooling) we observe a classical thermal shift behavior. Moreover, the $COP$ values decrease up to 2.34, which is extremely low and unrealistic. For the three other scenarios, the induced heat in the soil, during building cooling period, will help to prevent such behavior. Second, the $COP$ and $COP_S$ variation are extremely important. We can observe the importance of heat recharge of the soils during summer. Indeed, greater building cooling demand will lead to increase the soil temperature which will provide easier exploitation of heat power during winter, *i.e.* higher $COP$ value. However, even for high thermal recharge of the soil, heat exploitation will lead to rapidly decrease soil temperature and therefore decrease the $COP$ values.

Results of $COP$ and $COP$ values with $0.4\ \text{m}\cdot\text{day}^{-1}$ seepage are presented in Figure 10b. On this figure, we can observe a totally different behavior. Indeed, the systems exhibit similar behavior in each case. During summer, the cooling system exposes almost constant $COP_S$ value around 8.6. And during winter, the $COP$ factor varies from 4.2 to 5.2. Moreover, as expected, no scenario exposes multi-year thermal shift. These results could easily be explained by the thermal washing effect. Indeed, seepage phenomenon will tend to cancel thermal anomalies and impose an almost constant soil temperature around the energy piles, therefore the $COP$ and $COP_S$ variations are mainly related to the variation of heating and cooling demand.

Finally, Table 2 presents the average $COP$ value computed for each scenario during the winter period. As expected, the unbalanced scenario without seepage presents the lower average $COP$. In opposition, the fully balanced scenario without seepage shows the maximal average $COP$ (higher than seepage cases). This shows the beneficial aspect of heat storage mechanism during summer. However, this high average $COP$ conclusion should be mitigated by the important $COP$ variation observed. Scenarios with seepage will not benefit from heat storage effect. However, the thermal washing effect will guarantee constant and identical efficiency

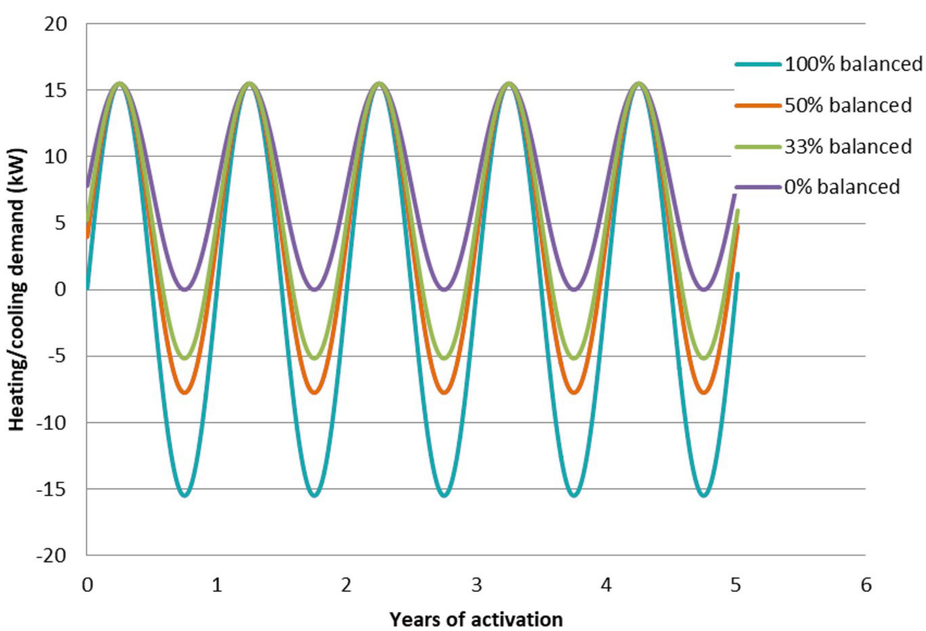


**Figure 9.** Heating/cooling seasonal scenarios.

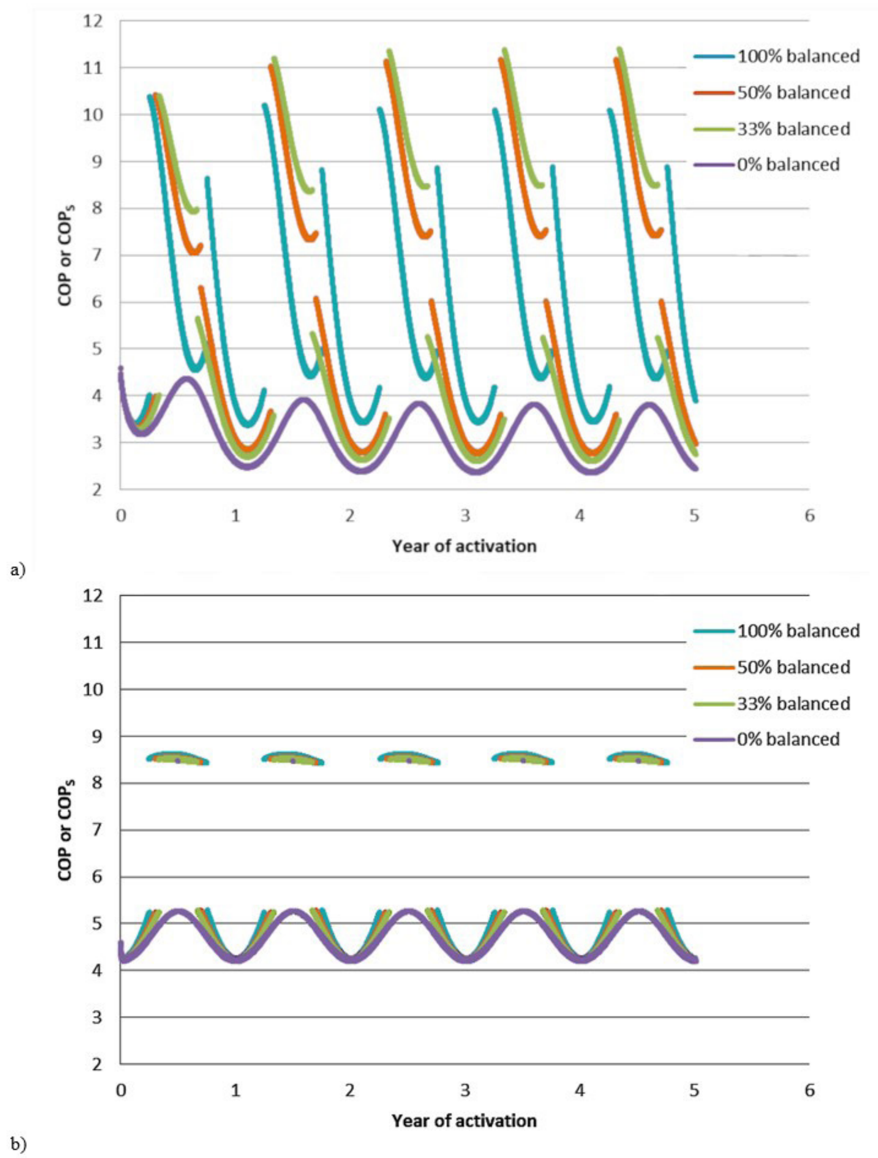


**Figure 10.** COP and $COP_S$ value for different scenarios; a) 0 $m \cdot day^{-1}$ seepage; b) $0.4 m \cdot day^{-1}$ seepage.

**Table 2.** Average COP during winter period for different scenarios.

| Seepage | 100% balanced | 50% balanced | 33% balanced | 0% balanced |
|---|---|---|---|---|
| 0 $m.day^{-1}$ | 4.79 | 3.62 | 3.34 | 3.03 |
| 0.4 $m.day^{-1}$ | 4.57 | 4.59 | 4.60 | 4.73 |

through multi-year activation, independently of balance in heating and cooling cycles. For a 50% balanced scenario, the average $COP$ is already better in the seepage case.

## 6. Conclusion, discussion and perspective

In this study, we present a numerical modelling process to represent energy geostructure behavior with the influence of seepage velocities and heating/cooling load depending on heat pump efficiency. This process allowed us to compute soil and system temperature, $COP$ and $COP_S$ factor variation depending on seepage conditions, geometrical aspects, and various heating/cooling scenarios.

With a first model, we present the behavior of a realistic energy pile group during one month of peak use (winter and summer), for various seepage conditions and various inter-pile distances. We show that in any case, the $COP$ (or $COP_S$ ) decreases during this month with soil temperature variation. However, the minimal value widely varies on the seepage condition and geometry. On one hand, the seepage condition has the most important effect on the $COP$ (or $COP_S$). It allows thermal washing and balance between energy inflow by advection effect and energy drained by the heat pump system. Therefore, seepage will conduct to a quick stabilization of the behavior, while slow or absent seepage will lead to continuous decreasing of $COP$ factor. On the other hand, the inter-pile distance will also influence the $COP$ values, as greater inter-pile distances will increase the heat reservoir size and reduce the cluster effect. Finally, as both parameters have an effect on the $COP$ factor, *i.e.*, the system efficiency, it could be estimated with the proposed expression (Equation 14).

With a second model, we present the behavior of the same system through multi-year solicitation with heating and cooling cycles, balanced and unbalanced, and two different seepage velocities. Again, the results show the importance of seepage conditions. It allows the stabilization of the behavior independently of the heating/cooling balance at reasonable efficiency level, but will not allow heat storage. In opposition, without seepage, the thermal recharge and heat storage (with building cooling for example) is particularly important in order to avoid the multi-year thermal shift and to increase the overall efficiency of the system. Accepting strong variation, the average $COP$ in cases with important heat storage could even be greater than cases with important seepage velocities condition.

These results are promising, and the process can easily be applied to various other cases. However, the heating/cooling scenario should be selected with care. Indeed, some purely hypothetical scenarios presented in this work will lead to soil temperatures so low that the realistic heat pump would turn off for safety reasons. Therefore, the presented process still could be improved. For example, emergency cases should be introduced to mitigate the use of heat-pump in cases of overconsumption of soil energy. Similarly, model description could also be improved, for example, with more detailed interaction at model boundaries or with thermal boundary condition depending on the depth.

In the future, the possibilities offered by this model should be used at a larger scale with more diverse scenarios. We plan to produce models with multiple heat pump systems with independent parameters and compute individual and global efficiency. We could also imagine developments to integrate other energy geostructures such as tunnels or walls and conventional geothermal systems (open loop, borehole, etc.).

## Acknowledgements

This work was supported by self-funding from University Gustave Eiffel. The authors report there are no competing interests to declare.

## Declaration of interest

The authors have no conflicts of interest to declare. All co-authors have observed and affirmed the contents of the paper and there is no financial interest to report.

## Authors' contributions

Thibault Badinier: conceptualization, data curation, visualization, writing – original draft. Badr Ouzzine: conceptualization, data curation, formal analysis. Jean de Sauvage: conceptualization, methodology, validation. Philippe Reiffsteck: supervision, validation.

## Data availability

The participants of this study did not give express written consent for their data to be shared publicly; therefore, due to the sensitive nature of the research, supporting data is only available upon request.

## Declaration of use of generative artificial intelligence

This work was prepared without the assistance of generative artificial intelligence

## List of symbols and abbreviations

$h, h_{min}, h_{max}$ Hydraulic charge, minimal and maximal value on limit condition [ $m$ ]
$k$ Water permeability [ $m.s^{-1}$ ]
$q$ heat transfer fluid pumping rate [ $m^3.s^{-1}$ ]
$t$ time
$D$ Inter-pile distance [ $m$ ]
$C_v$ , $C_{v,f}$ , $C_{v,w}$ Volumetric heat capacity, specific parameters for heat transfer fluid and water [ $W.s.m^{-3}.K^{-1}$ ]
$COP$ , $COP_S$ Heat pump performance coefficient and for summer mode [ 1 ]
$COP_{max}$ Target COP value for analytical evaluation [1]
$\vec{j}$ , $\vec{j}_{adv}$ , $\vec{j}_{cond}$ Total, advective and, convective heat flux [ $W$ ]
FEM Finite Element Modelling
$Q_{cold}$ , $Q_{cold,S}$ Power exchange on cold source and for summer mode [ $W$ ]
$Q_{hot}$ , $Q_{hot,S}$ Power exchange on hot source and for summer mode [ $W$ ]
$R_{th}$ Thermal resistance of the pile per meter [ $K.W^{-1}$ ]
$T$ Temperature [ $K$ ]
$T_{cold}$ , $T_{cold,S}$ Temperature on cold source and for summer mode [ $K$ ]
$T_{edge}$ Temperature on limit condition [ $K$ ]
$T_{hot}$ , $T_{hot,S}$ Temperature on hot source and for summer mode [ $K$ ]

$T_{fl}$ Average heat transfer fluid temperature [K]
$T_{in}, T_{out}$ Inlet and outlet temperature on cold circuit [K]
$T_{init}$ Initial soil temperature [ $K$ ]
$W$ Heat pump electric power consumption [ $W$ ]
$\lambda$ Thermal conductivity [ $W.m^{-1}.K^{-1}$ ]
$\vec{v}$ Darcy seepage Velocity [ $m.s^{-1}$ ]

## References


Abu-Hamdeh, N.H. (2003). Thermal properties of soils as affected by density and water content. *Biosystems Engineering*, *86*(1), 97-102. http://doi.org/10.1016/S1537-5110(03)00112-0.

Allaerts, K., Coomans, M., & Salenbien, R. (2015). Hybrid ground-source heat pump system with active air source regeneration. *Energy Conversion and Management*, *90*, 230-237. http://doi.org/10.1016/j.enconman.2014.11.009.

Amatya, B., Soga, K., Bourne-Webb, P., Amis, T., & Laloui, L. (2012). Thermo-mechanical behaviour of energy piles. *Geotechnique*, *62*(6), 503-519. http://doi.org/10.1680/geot.10.P.116.

Anstett, M., Hubbuch, M., Laloui, L., Matthey, B., Morath, M., Pahud, D., Parriaux, A., Rybach, L., Schönbächler, M., Tacher, L., & Wilhelm, J. (2005). *Utilisation de la chaleur du sous-sol par des ouvrages de fondation et de soutènement en béton – Guide pour la conception, la réalisation et la maintenance* [Report]. University of Applied Sciences and Arts of Southern Switzerland. (in French). Retrieved in May 30, 2024, from https://repository.supsi.ch/3052/

Attard, G., Rossier, Y., Winiarski, T., & Eisenlohr, L. (2016). Deterministic modeling of the impact of underground structures on urban groundwater temperature. *The Science of the Total Environment*, *572*, 986-994. http://doi.org/10.1016/j.scitotenv.2016.07.229.

Badinier, T., de Sauvage, J., Ouzzine, B., Szymkiewicz, F., Reiffsteck, P., Delerablée, Y., & Minatchy, C. (2023). Energy geostructure: experimental and numerical modelling of thermal behaviour and interaction within the city underground. *European Journal of Environmental and Civil Engineering*, *27*(15), 4396-4415. http://doi.org/10.1080/19648189.2023.2191120.

Badinier, T., Ghandri, I., Grappe, T., Ouzzine, B., & de Sauvage, J. (2022). Géostructures thermiques\hspace0.167em : verrous scientifiques et moyens d'étude. *Revue Française de Géotechnique*, *172*, 1. http://dx.doi.org/10.1051/geotech/2022007.

Barla, M., Di Donna, A., & Baralis, M. (2018). City-scale analysis of subsoil thermal conditions due to geothermal exploitation. *Environmental Geotechnics*, *7*(4), 306-316. http://doi.org/10.1680/jenge.17.00087.

Barla, M., Di Donna, A., & Insana, A. (2019). A novel real-scale experimental prototype of energy tunnel. *Tunnelling and Underground Space Technology*, *87*, 1-14. http://doi.org/10.1016/j.tust.2019.01.024.

Bourne-Webb, P., Burlon, S., Javed, S., Kürten, S., & Loveridge, F. (2016). Analysis and design methods for energy geostructures. *Renewable & Sustainable Energy Reviews*, *65*, 402-419. http://doi.org/10.1016/j.rser.2016.06.046.

Brach, A., Balliere, A., Heumez, S., Jeanpierre, F., Laheurte, P., Landry, B., & Legrand, S. (2014). *Eurocode 7; Application Aux Fondations Profondes (NF P94-262)* [Report] Cerema (in French).

Brandl, H. (2006). Energy foundations and other thermo-active ground structures. *Geotechnique*, *56*(2), 81-122. http://doi.org/10.1680/geot.2006.56.2.81.

Burlon, S., Desodt, C., Habert, J., & Reiffsteck, P. (2017). *Calcul des ouvrages géotechniques selon l'Eurocode 7*. Dunod (in French).

Cecinato, F., & Loveridge, F.A. (2015). Influences on the thermal efficiency of energy piles. *Energy*, *82*, 1021-1033. http://doi.org/10.1016/j.energy.2015.02.001.

CFMS, Syntec Ingénierie & SOFFONS-FNTP. (2017). *Recommandations pour la conception, le dimensionnement et la mise en œuvre des géostructures thermiques* [Report]. CFMS. (in French).

CFMS. (2022). *Webinaire CFMS - Produire de l'énergie avec les géostructures thermiques* [Presentation] (in French). Retrieved in May 30, 2024, from https://youtu.be/NQobXjIycPs?si=aZrkUCSW12JYy2QQ

Cui, Y., & Zhu, J. (2018). CFD assessment of multiple energy piles for ground source heat pump in heating mode. *Applied Thermal Engineering*, *139*, 99-112. http://doi.org/10.1016/j.applthermaleng.2018.04.073.

de Sauvage, J., Badinier, T., Sauvage, J., Szymkiewicz, F., & Benitez, B. R. (2020). Groupe de pieux thermoactifs dans un écoulement aquifère: modélisation physique et numérique. In *Proceedings of Journées Nationales de Géotechnique et de Géologie de l'Ingénieur – Lyon 2020* (pp. 1-9). Lyon, France. (in French).

Delerablée, Y. (2019). *Intégration thermique et mécanique des géostructures thermiques: de l'échelle du bâtiment à l'échelle de la cité* [Doctoral thesis, Université Paris Est]. Université Paris Est (in French).

Di Donna, A., Barla, M., & Amis, T. (2017, octobre 19). Energy geostructures: a collection of data from real applications. In *Proceedings of 15th IACMAG*. China.

Di Donna, A., Emeriault, F., Demongodin, L., & Gobichon, J.-F. (2020). Aspects géotechniques et énergétiques des géostructures thermoactives: application à un cas d'étude réel. *Revue Française de Géotechnique*, *164*, 4. (in French).

Di Donna, A., Loria, A.F.R., & Laloui, L. (2016). Numerical study of the response of a group of energy piles under different combinations of thermo-mechanical loads. *Computers and Geotechnics*, *72*, 126-142. http://doi.org/10.1016/j.compgeo.2015.11.010.

Fadejev, J., Simson, R., Kurnitski, J., & Haghighat, F. (2017). A review on energy piles design, sizing and modelling. *Energy*, *122*, 390-407. http://doi.org/10.1016/j.energy.2017.01.097.

Fadejev, J., Simson, R., Kurnitski, J., Kesti, J., Mononen, T., & Lautso, P. (2016). Geothermal heat pump plant performance in a nearly zero-energy building. *Energy Procedia*, *96*, 489-502. http://doi.org/10.1016/j.egypro.2016.09.087.

Frodl, S., Franzius, J.N., & Bartl, T. (2010). Design and construction of the tunnel geothermal system in Jenbach. *Geomechanics and Tunnelling*, *3*(5), 658-668. http://doi.org/10.1002/geot.201000037.

Fromentin, A., & Pahud, D. (1997). *Recommandations pour la réalisation d'installations avec pieux échangeurs* [Report]. Office Fédéral de l'énergie (in French).

Fujii, H., Itoi, R., Fujii, J., & Uchida, Y. (2005). Optimizing the design of large-scale ground-coupled heat pump systems using groundwater and heat transport modeling. *Geothermics*, *34*(3), 347-364. http://doi.org/10.1016/j.geothermics.2005.04.001.

Gultekin, A., Aydin, M., & Sisman, A. (2016). Thermal performance analysis of multiple borehole heat exchangers. *Energy Conversion and Management*, *122*, 544-551. http://doi.org/10.1016/j.enconman.2016.05.086.

Humbert, P., Dubouchet, A., Fezans, G., & Remaud, D. (2005). CESAR-LCPC, un progiciel de calcul dédié au génie civil. *Bulletin des Laboratoires des Ponts et Chaussées*, *256*, 7-37 (in French).

International Energy Agency – IEA. (2022). *Energy statistics data browser*. Retrieved in May 30, 2024, from https://www.iea.org/data-and-statistics/data-tools/energy-statistics-data-browser

Laloui, L., & Di Donna, A. (2013). *Energy geostructures: innovation in underground engineering*. John Wiley & Sons.. http://doi.org/10.1002/9781118761809.

Lazzari, S., Priarone, A., & Zanchini, E. (2010). Long-term performance of BHE (borehole heat exchanger) fields with negligible groundwater movement. *Energy*, *35*(12), 4966-4974. http://doi.org/10.1016/j.energy.2010.08.028.

Li, C., Cleall, P.J., Mao, J., & Muñoz-Criollo, J.J. (2018). Numerical simulation of ground source heat pump systems considering unsaturated soil properties and groundwater flow. *Applied Thermal Engineering*, *139*, 307-316. http://doi.org/10.1016/j.applthermaleng.2018.04.142.

Lou, Y., Fang, P., Xie, X., Chong, C.S.A., Li, F., Liu, C., Wang, Z., & Zhu, D. (2021). Numerical research on thermal response for geothermal energy pile groups under groundwater flow. *Geomechanics for Energy and the Environment*, *28*, 100257. http://doi.org/10.1016/j.gete.2021.100257.

Loveridge, F., McCartney, J.S., Narsilio, G.A., & Sanchez, M. (2020). Energy geostructures: a review of analysis approaches, in situ testing and model scale experiments. *Geomechanics for Energy and the Environment*, *22*, 100173. http://doi.org/10.1016/j.gete.2019.100173.

Maghsoodi, S. (2020). *Thermo-mechanical behavior of soil-structure interface under monotonic and cyclic loads in the context of energy geostructures* [Doctoral thesis, Université de Lorraine]. Université de Lorraine.

Makasis, N., & Narsilio, G.A. (2020). Energy diaphragm wall thermal design: the effects of pipe configuration and spacing. *Renewable Energy*, *154*, 476-487. http://doi.org/10.1016/j.renene.2020.02.112.

Mimouni, T., & Laloui, L. (2015). Behaviour of a group of energy piles. *Canadian Geotechnical Journal*, *52*(12), 1913-1929. http://doi.org/10.1139/cgj-2014-0403.

Ouzzine, B., Sauvage, J., Madabhushi, G., Viggiani, G., & Reiffsteck, P. (2023). Centrifuge modelling of an energy pile group with groundwater flow. *International Journal of Physical Modelling in Geotechnics*, *24*(3), 150-160. https://doi.org/10.1680/jphmg.22.00041.

Pahud, D. (2013). A case study: the dock midfield of zurich airport. In L. Laloui & A. Di Donna (Eds.), *Energy geostructures: innovation in underground engineering* (pp. 281-296). Wiley-ISTE.

Pahud, D., & Hubbuch, M. (2007). Measured thermal performances of the energy pile system of the dock midfield at Zürich Airport. In *Proceedings of European Geothermal Congress 2007* (pp. 1-7). Unterhaching, Germany.

Pahud, D., & Lachal, B. (2004). *Monitoring the thermal performance of a heat pump coupled to geothermal probes at Lugano (Switzerland); Mesure des performances thermiques d'une pompe a chaleur couplee sur des sondes geothermiques a Lugano (TI)*. [Report]. Office Fédéral de l'énergie (in French).

Piau, J.-M., Mainguy, M., & Magnan, J.-P. (2005). *CESAR-LCPC, Référentiel Théorique, Les Modules de Diffusion Non Linéaire DTNL, NAPP Et NSAT* [Report]. LCPC.

Staffell, I., Brett, D., Brandon, N., & Hawkes, A. (2012). A review of domestic heat pumps. *Energy & Environmental Science*, 5(11), 9291-9306. http://doi.org/10.1039/c2ee22653g.

Yavari, N. (2014). *Aspects géotechniques des pieux de fondation énergétiques* [Doctoral thesis, Université Paris Est]. Université Paris Est (in French).

Zanchini, E., Lazzari, S., & Priarone, A. (2012). Long-term performance of large borehole heat exchanger fields with unbalanced seasonal loads and groundwater flow. *Energy*, *38*(1), 66-77. http://doi.org/10.1016/j.energy.2011.12.038.

Zhao, Z., Lin, Y.-F., Stumpf, A., & Wang, X. (2022). Assessing impacts of groundwater on geothermal heat exchangers: a review of methodology and modeling. *Renewable Energy*, *190*, 121-147. http://doi.org/10.1016/j.renene.2022.03.089.